Scattering and nonlinear bound states of hydrodynamically coupled particles in a narrow channel

William E. Uspal[1] and Patrick S. Doyle[2]
[1]*Department of Physics, Massachusetts Institute of Technology, Cambridge, Massachusetts 02139, USA*
[2]*Department of Chemical Engineering, Massachusetts Institute of Technology, Cambridge, Massachusetts 02139, USA*
(Received 7 June 2011; revised manuscript received 19 December 2011; published 27 January 2012)

We model a pair of hydrodynamically interacting particles confined in a channel with thin rectangular cross section. We find that the particles have a finite region of attraction, which arises from the screening of dipolar hydrodynamic interactions by the side walls. Outside this region, the two particles break apart and scatter; inside, they oscillate together as an effectively free quasiparticle. We demonstrate that modulation of channel geometry provides a means to irreversibly manipulate bound pairs.

DOI: 10.1103/PhysRevE.85.016325 PACS number(s): 47.15.G−, 47.57.−s, 47.61.−k

I. INTRODUCTION

Control of flowing suspensions of particles is central to many emerging microfluidic applications, including cell sorting [1], information processing [2], and assembly of complex structures [3]. If the desired colloidal manipulations could be encoded directly into the microchannel geometry, they could be performed sequentially, continuously, and with high throughput. Recently, researchers have investigated self-organized states and nonlinear dynamics arising from hydrodynamic interactions between colloidal particles [4,5]. These interactions are dramatically sensitive to geometric confinement. For instance, it has been shown that *Volvox* algae colonies swimming near a plane wall form oscillatory bound pairs [6]. Between parallel plates, a flowing linear train of droplets can support longitudinal and transverse acoustic waves, owing to the unique dipolar form of hydrodynamic interactions in this geometry [7]. Likewise, this dipolar form leads to the formation of patterns [8] and sharp interfaces [9] in confined particle arrays.

In this paper, we model the dynamics of a particle pair confined to a channel of thin rectangular cross section. We show numerically that the interplay of the dipolar form and the screening of hydrodynamic interactions by the side walls gives rise to two behaviors: scattering, in which pair distance grows without bound, or nonlinear oscillations, for which pair distance remains bounded. The oscillations take place far from equilibrium, as the energy provided by the external flow is dissipated by viscosity in this overdamped system. Nevertheless, they retain surprising similarity to free oscillations in a conservative system, owing to the time reversal symmetry of the underlying equations [10]. We characterize the observed behavior as due to an effective softening spring nonlinearity and, drawing on this analogy to a finite potential well, we show that a resonant, long wavelength perturbation to the channel boundaries can chaotically break oscillatory pairs. Our results demonstrate that irreversible particle manipulations can be performed through patterning of confining boundaries.

II. MODEL

Consider a particle confined between infinite parallel plates. If the characteristic particle size L is comparable to the height of the slit H, its motion is confined to a plane. When the particle moves with respect to the surrounding fluid, it creates an in-plane disturbance field with a long-range dipolar form [11]. This form arises from mass conservation: because of friction from the confining walls, the flux of momentum from a force multipole is exponentially screened over a length scale set by the slit height H. Lack of momentum conservation fundamentally distinguishes this "quasi-two-dimensional" (q2D) system from genuine 2D Stokes flow [12]. The velocity field will have an approximate parabolic dependence in the z (plate normal) direction, determining the areal density of the force of friction on the fluid as $\gamma_c H \mathbf{U}(\mathbf{r})$, where $\gamma_c = 8\mu/H^2$, μ is the bulk dynamic viscosity, and $\mathbf{U}(\mathbf{r})$ is the fluid velocity relative to the channel walls at a point $\mathbf{r}$ in the midplane $z = H/2$. The friction on the particle, determined by the details of the lubricating fluid that separates the particle from the walls, can be associated with a parameter γ_p. This coefficient will in general be higher than γ_c, so that, in an external flow, the particle will not be freely advected but lag the surrounding fluid and create a dipolar disturbance field.

Now we consider a collection of N such particles. We can approximate the velocity field $\mathbf{U}(\mathbf{r}_i)$ at particle i as the external field plus the disturbance created by the other particles and, neglecting velocity gradients, we can use the drag coefficient ζ for a cylindrical particle of radius $R = L/2$ in a q2D uniform flow, as discussed in the appendix. This gives a system of $2N$ equations for force-free particles:

$$\gamma_c \pi R^2 H \mathbf{U}(\mathbf{r}_i) - \gamma_p \pi R^2 H \mathbf{U}_i^p + \zeta\left[\mathbf{U}(\mathbf{r}_i) - \mathbf{U}_i^p\right] = 0, \qquad (1)$$

where $\mathbf{U}_i^p$ is the velocity of particle i relative to the channel walls and $\mathbf{r}_i = (x_i, y_i)$ is its position in the fixed coordinate system of Fig. 1(a). Assuming a uniform external flow $\mathbf{U}_0 = U_0\hat{x}$, the local field is evaluated to leading order in r_{ij}:

$$\mathbf{U}(\mathbf{r}_i) = \mathbf{U}_0 + \sum_j \mathbf{V}^{(ij)}(\mathbf{r}_{ij}) \cdot \left(\mathbf{U}_j^p - \mathbf{U}_0\right), \qquad (2)$$

where $\mathbf{V}^{(ij)}(\mathbf{r}_{ij})$ is a tensor determining the contribution of particle j to the local field at i, detailed in the Appendix, and $\mathbf{r_{ij}} \equiv \mathbf{r}_j - \mathbf{r}_i$. These equations can be rearranged into matrix form, $\mathbf{A}\mathbf{U}^p = \mathbf{B}$, where $\mathbf{U}^p$ is a vector containing the $2N$ particle velocities. The off-diagonal terms in the resistance matrix $\mathbf{A}$ represent the coupling between particles, while terms involving the external flow $\mathbf{U}_0$ are collected in the vector $\mathbf{B}$. Numerically, we can solve the N-particle problem by forming $\mathbf{A}$ and $\mathbf{B}$ at each time step, inverting $\mathbf{A}$ to obtain $\mathbf{U}^p$, and integrating forward in time via a Runge-Kutta routine. While

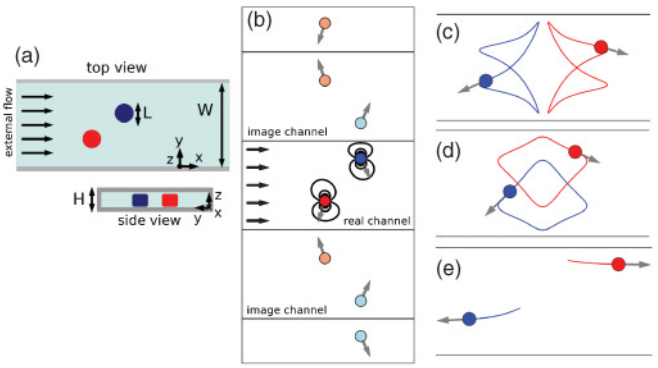

FIG. 1. (Color online) (a) Particles of length L are confined to two-dimensional motion in a channel of width W and height H, where $H < L < W$ and subject to an external flow. (b) Top-down view of the system of images used to impose the no-mass flux condition at the channel side walls. The real particles (dark red and dark blue) are dressed by an infinite set of images (light colors). The particles lag the external flow and are therefore coupled by dipolar flow disturbance fields. Gray vectors are particle velocities in a frame moving with the x component of the particles' center of mass, $x_{\text{c.m.}}$. (c) Particle trajectories in the $x_{\text{c.m.}}$ frame for oscillation around a 0° fixed point, as described in the text. (d) Particle trajectories around a 90° fixed point. (e) A scattering event.

A is populated only by single and two-body terms, its inversion solves a many-body problem.

In this geometry, the two-body problem is analytically trivial: we obtain that $\mathbf{r}_{12}$ is fixed, and that the particles have a component of velocity perpendicular to the external flow $U^p_{1,y} \sim U_0 \sin(\theta_{12})\cos(\theta_{12})$, where θ_{12} is the angle between $\mathbf{r}_{12}$ and $\mathbf{U}_0$, analogous to a pair of widely separated sedimenting particles in unbounded three-dimensional (3D) fluid. Clearly, with an additional set of confining side walls, a pair cannot indefinitely maintain constant velocity in y. To introduce side walls, we draw on an analogy with 2D electrostatics and enforce the no-mass flux boundary condition via a set of images [Fig. 1(b)]. The side walls are separated by a distance W, and each particle is dressed by an infinite set of reflections. By performing the appropriate summations, we obtained the dressed self- and two-particle contributions to the hydrodynamic interaction tensor, detailed in the appendix. Significantly, the reflections exponentially screen two-particle coupling in the channel direction x over a length scale $\sim W$ [13]. We note that our expression for the disturbance velocity created by motion in the x direction reduces to an expression obtained for a quasi-one-dimensional channel, Eq. (1) in Ref. [13], in the limit that $\gamma \to 0$. This limit represents the neglect of fluid incompressibility (i.e., the effect of channel blockage by a finite-sized particle). However, this effect is not significant for the channel sizes we consider. The thin channel approximation allows us to neglect the effects of particle rotation and shear layers near solid boundaries. We have explored including all reflections in evaluation of the local field [i.e., replacing the second $\mathbf{U}_0$ in Eq. (2) with $\mathbf{U}(\mathbf{r}_j)$], but the quantitative effect was insignificant.

Our model is a minimalistic representation of hydrodynamically coupled particles as coupled dipolar flow singularities, reducing the full set of partial differential equations for the flow field to a set of $2N$ coupled ordinary differential equations. Such "singularity" models have been applied to systems of vortices, swimmers, and sedimenting particles [10,14–16]. The simplicity of such models permits rapid identification of dynamical motifs sustained by hydrodynamics, which can then be studied in detail via experiments or more fully featured simulations. For instance, the main results for sedimentation of coupled Stokeslets [15] were recovered in multipole simulations that included finite-size effects and lubrication interactions [17].

III. RESULTS

Numerically, we address the $N = 2$ problem with parameters $W = 8L$, $\gamma_p/\gamma_c = 25$, and ζ obtained from $H/L = 2/3$. Variation of these parameters did not significantly affect the dynamics we report. We sweep over initial particle configurations $(y_1, y_2, \Delta x)$, where Δx is separation in the flow direction, $\Delta x \equiv x_2 - x_1$. The angles $\theta_{12} = 0°$ and $\theta_{12} = 90°$ still constitute fixed points when $y_{\text{c.m.}} = W/2$, where $y_{\text{c.m.}} \equiv (y_1 + y_2)/2$, consistent with the symmetry in y. Otherwise, depending on the initial configuration, the two particles either oscillate around a 0° or 90° fixed point, remaining always together, or break apart and scatter, with $|\Delta x|$ growing without bound (Fig. 2). Owing to the time-reversal symmetry [10] of the underlying equations, the oscillations are closed loops in phase space. When particle trajectories are plotted in the frame moving with $x_{\text{c.m.}} \equiv (x_1 + x_2)/2$, they generically resemble Figs. 1(c) and 1(d): two figure eights for 0° and two loops (which do not necessarily cross) for 90°. We distinguish scattering trajectories as having a final $|\Delta x| > 2W$. Invoking time-reversal symmetry, we see that these trajectories are pieces of longer trajectories, symmetric around $\Delta x = 0$, for particles that start with $\Delta x = \pm\infty$, approach and interact near $\Delta x = 0$, and scatter to $\Delta x = \mp\infty$. Robust bound states are possible only for particles that are initially close together,

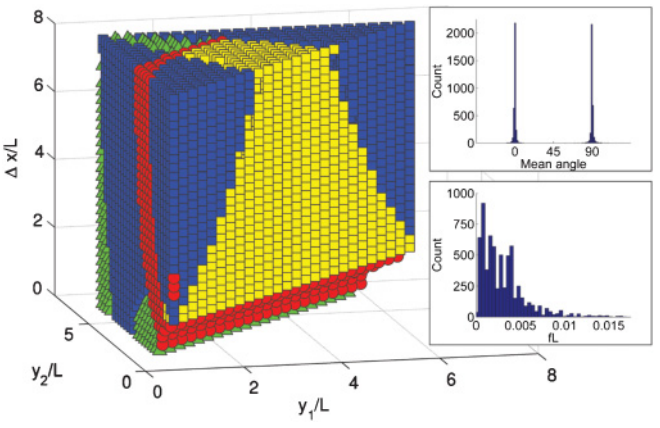

FIG. 2. (Color online) Phase map indicating behavior for the initial condition $(y_1, y_2, \Delta x)$. Yellow (light) squares indicate oscillation around a 0° fixed point; green (light) triangles, a 90° fixed point; blue (dark) squares, scattering; and red (medium) circles, particle-particle or particle-wall overlap. For the oscillatory trajectories, the inset figures show the distributions of mean angle and frequency, where fL is found by taking the spatial Fourier transform, as described in the text.

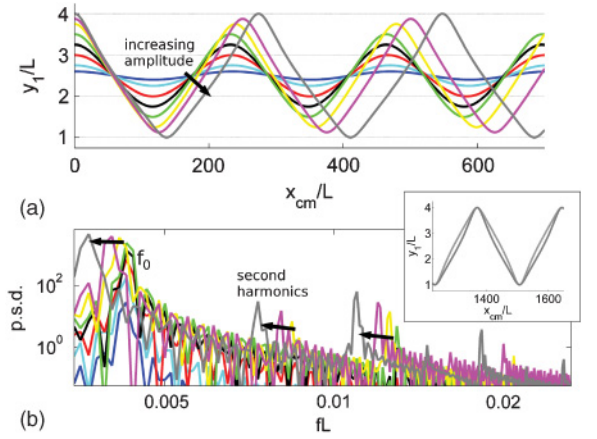

FIG. 3. (Color online) (a) Position of particle in y with $x_{\text{c.m.}}$ for initial separation $\Delta y = 3L$ and $\Delta x = 0$ and various initial displacements of $y_{\text{c.m.}}$ from the centerline, where the fixed point has $y_1/L = 2.5$. (b) Matched by color, the power spectra of the trajectories in (a), where f has units of inverse length. f_0 is predicted by linear theory. Arrows indicate the shift of peaks with increasing amplitude. The appearance of second harmonics is linked to the breaking of the half-wave symmetry $y_1(x_{\text{c.m.}} + \lambda/2) - 2.5L = -[y_1(x_{\text{c.m.}}) - 2.5L]$, where λ is the signal wavelength. The inset shows both the largest amplitude trajectory from (a) and the result of performing the symmetry operation on it; the curves do not coincide.

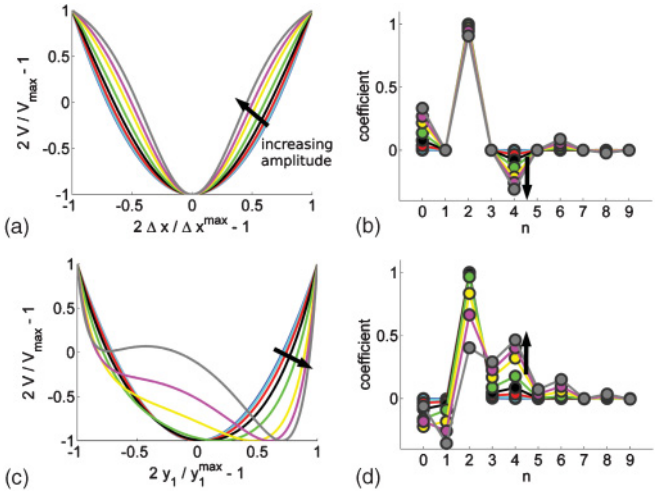

FIG. 4. (Color online) Effective potentials in Δx (a) and y_1 (c) for the trajectories in Fig. 3, matched by color. The potentials are shifted and rescaled for characterization in the Chebyshev basis. (b) For motion in Δx, a negative coefficient of T_4 for large-amplitude oscillations indicates a softening nonlinearity. (d) For motion in y_1, large-amplitude oscillations have skewed potentials, consistent with the half-wave symmetry breaking. Arrows indicate the effect of increasing amplitude.

$|\Delta x| < 2W$. Finally, we reject trajectories in which particles overlap with each other or with the side walls. While we could eliminate overlap via the inclusion of lubrication or contact forces, we are primarily interested in the effect of far-field hydrodynamics.

In order to examine the nonlinear oscillations in detail, we consider a pair of particles with initial separation $\Delta x = 0$ and $\Delta y = 3L$, where $\Delta y \equiv y_2 - y_1$. When $y_{\text{c.m.}}$ is on the channel centerline, the pair is at a fixed point and only translates in the flow direction. If the initial $y_{\text{c.m.}}$ is displaced from the centerline for fixed initial separation, the pair will oscillate around a 90° fixed point with amplitude in y identical to the magnitude of the initial displacement. Since time can be arbitrarily rescaled when $\text{Re} = 0$, we consider the variation of y_1/L with $x_{\text{c.m.}}/L$ instead of with time [Fig. 3(a)]. The small-amplitude signals are sinusoidal, well described by linearization about the fixed point, while large-amplitude signals are nearly triangular. The power spectra, determined by spatially Fourier transforming the trajectories in Fig. 3(a), reveal a shift in the fundamental frequency with amplitude, as well as growth in odd and, eventually, even harmonics [Fig. 3(b)]. As shown in the inset, the appearance of even harmonics is the signature of broken half-wave symmetry. This symmetry breaking can be attributed to the strong interaction of a particle with its nearest image in the vicinity of a wall. The nearest image retards motion in y, since the component of its velocity in y is opposite that of the original particle.

Since the oscillations are closed loops in phase space, they resemble free motion in a conservative potential. We define an effective potential in coordinate q as $V_q = -\dot{q}^2$. For 90° oscillations, potentials defined via coordinates y_i and Δx are single valued. In Fig. 4, we shift and rescale the effective potentials for the trajectories of Fig. 3 in order to characterize their shapes via projection onto a basis set of Chebyshev polynomials. For the potential defined in Δx, a softening nonlinearity is indicated by growth in a negative coefficient of the fourth Chebyshev polynomial $T_4(x) \equiv 8x^4 - 8x^2 + 1$ with increasing amplitude of oscillation. All oscillatory trajectories have $\partial V/\partial|\Delta x| \geqslant 0$. If a trajectory could explore the region where $\partial V/\partial|\Delta x| < 0$, then $|\Delta x|$ would grow without bound, which would be observed as a scattering event. This softening can be attributed to the weakening of the pair interaction in $|\Delta x|$ by the side walls.

The finitude of the effective potential suggests that, if a particle pair could explore its effective potential diffusively, it might unbind stochastically. Since the fixed point of oscillations is at the channel centerline, a sinusoidal pattern that displaces the side walls (varying the walls' position in y with x, but not with time, and fixing W) recalls parametric variation of a spring tether point—a route to chaotic escape for finite potential oscillators. For a configuration with initial separation $\Delta y = 3L$ and $\Delta x = 0$, as previously considered, and $y_{\text{c.m.}}$ initially on the the centerline, $y_{\text{c.m.}} = W/2$, we vary the amplitude A/L and spatial frequency f_w/f_0 of a wall perturbation. Without a wall perturbation, this configuration is a fixed point. f_0 is the fundamental frequency of small-amplitude oscillations, shown in Fig. 3. The wavelength of the perturbation $\lambda_w = f_w^{-1}$ is always large, $\lambda_w \gg W > L$, such that we can retain the model developed for straight walls. For each set of parameters, we perform ten simulations for a dimensionless time $7.5 \times 10^4\ L/U_0$, with each trajectory initially perturbed in phase space by noise with magnitude $\epsilon = 10^{-4}$. We calculate the Euclidean distance of each trajectory with respect to a reference trajectory. Taking scattered trajectories to have a final $|\Delta x| > 2W$, we define the

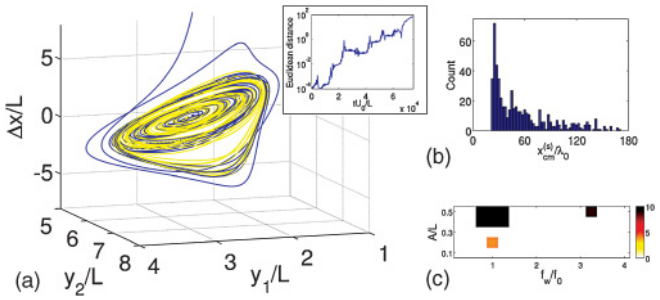

FIG. 5. (Color online) (a) Phase portrait of two trajectories with $A/L = 0.2$ and $f_w/f_0 = 1$ initially separated by a noise vector in phase space with magnitude $\epsilon = 10^{-4}$. The trajectories diverge exponentially (inset). (b) Distribution of scattering length $x^{(s)}_{\text{c.m.}}$ for $A/L = 0.2$ and $f_w/f_0 = 1$. (c) Number of scattering and overlap trajectories for various amplitudes and spatial frequencies of a sinusoidal pattern. The results for irrational frequency ratios are similar.

scattering distance $x^{(s)}_{\text{c.m.}}$ as the minimum $x_{\text{c.m.}}$ for which this criterion is satisfied.

We find that while most trajectories remain bound states, a finite-amplitude perturbation at a resonant wavelength can lead to chaotic scattering. Scattering and overlap trajectories are clustered around $f_w/f_0 = 1$ [Fig. 5(c)]. The scattering trajectories are chaotic, diverging exponentially from the reference trajectories [Fig. 5(a)]. For $A/L = 0.1, A/L = 0.2$, and $A/L = 0.5$ at $f_w/f_0 = 1$, we run an additional set of one thousand trajectories to probe stability and the distribution of scattering length. None of the most weakly perturbed trajectories scattered. This suggests that experimental realizations of bound pairs would be robust against imperfections in channel geometry. The distribution of scattering lengths for $A/L = 0.2$ is shown in Fig. 5(b). Although the particles are non-Brownian, both the abrupt rise on the left and the long tail on the right are typical features of a distribution of first passage times for a diffusive particle with absorbing boundary. For $A/L = 0.5$, particles scatter quickly, accumulating little distance in phase space, so that $x^{(s)}_{\text{c.m.}}$ is strongly peaked around $x^{(s)}_{\text{c.m.}}/\lambda_0 = 5.3$, where $\lambda_0 = f_0^{-1}$. We note that time reversing the above-described scattering trajectories produces solutions in which particles are initially widely separated but induced to approach and form bound states, whereas robust bound states in the straight wall system required an initial $|\Delta x| < 2W$. Therefore, patterned walls can function either to release bound pairs or to trap initially free particles.

IV. CONCLUSION

In summary, we have shown that particles driven by an external flow in a narrow channel can form bound states when coupled through boundary-mediated hydrodynamic interactions. Owing to time-reversal symmetry, the bound state resembles a free "quasiparticle," oscillating in an effective potential constituted by the confining boundaries and the colloids own motion. The softening nonlinearity of this potential arises from the screening of interactions in the flow direction by the side walls. This softening limits pair binding to a finite region, outside of which the particles scatter to infinity. Patterning the confining boundaries for modulation of the hydrodynamic interaction provides a means to irreversibly trap, manipulate, and release colloidal particles without the application of external forces.

ACKNOWLEDGMENTS

This work was supported by the Institute for Collaborative Biotechnologies through contract No. W911NF-09-D-0001 from the US Army Research Office.

APPENDIX

A cylindrical particle with radius R and velocity $\mathbf{U}_i^p$ that is confined in a slit and subject to an external flow $\mathbf{U}$ which is uniform in the midplane can be modeled by the 2D Brinkman equation,

$$-\nabla P_{2D} + \mu_{2D}\nabla^2\mathbf{u} - \mu H a^2\mathbf{u} = 0, \tag{A1}$$

with $\nabla\cdot\mathbf{u} = 0$, where $a^2 \equiv 8/H^2$, $\mu_{2D} \equiv \mu H$, and $\mathbf{u}$ is the fluid velocity in the midplane. P_{2D} is the 2D pressure and has units of surface tension. The solution to this equation determines both the drag coefficient ζ [18] and the hydrodynamics interaction tensor $\mathbf{V}^{(ij)}_{\alpha\beta}$. The latter should be read as "the disturbance at particle i in direction α due to motion of particle j in direction β." The drag coefficient is

$$\zeta = 4\pi\mu_{2D}\left(\frac{a^2R^2}{4} + \frac{aRK_1(aR)}{K_0(aR)}\right). \tag{A2}$$

The force on the particle from the flow is

$$\mathbf{F} = \pi R^2\gamma_c H\mathbf{U} + \zeta\left(\mathbf{U} - \mathbf{U}_i^p\right). \tag{A3}$$

The first term in Eq. (A3) breaks Galilean invariance and arises from the external pressure gradient required to drive the flow against friction from the walls. Equation (1) is obtained after including the friction on the particle.

Retaining only the far-field, dipolar term, the hydrodynamics interaction tensor is xy symmetric and nonzero only for $i \neq j$:

$$\begin{aligned} B &\equiv \left(1 + \frac{2K_1(aR)}{aRK_0(aR)}\right)R^2, \\ X &\equiv (x_i - x_j), \quad Y \equiv (y_i - y_j), \\ V^{(ij)}_{xx} &= B(X^2 - Y^2)/r^4_{ij}, \quad V^{(ij)}_{xy} = 2BXY/r^4_{ij}, \\ V^{(ij)}_{yx} &= V^{(ij)}_{xy}, \quad V^{(ij)}_{yy} = -V^{(ij)}_{xx}. \end{aligned}$$

In a channel, particle i will not only interact with other particles, but also with its own images and the images of other particles. A particle and its images can be divided into two sets. The first set, designated "far," includes the original particle, as well as periodic images displaced from the original particle in the y direction with periodicity $2W$. The "near" set is seeded from the original particle's mirror image across the closest side wall and includes periodic copies of this image. The "near" set is so named because it includes the image closest to the original particle, and the $\hat{y}$ component of velocities in this set are negated relative to the original particle [Fig. 1(b)]. Summing over the images in these two sets, the self-interaction

$(i = j)$ is determined to be

$$C \equiv \left(1 + \frac{2K_1(aR)}{aRK_0(aR)}\right)\left(\frac{R\pi}{2W}\right)^2,$$
$$V^{(ii)}_{xx,\mathrm{far}} = -C/3, \quad V^{(ii)}_{yy,\mathrm{far}} = -V^{(ii)}_{xx,\mathrm{far}},$$
$$V^{(ii)}_{xy,\mathrm{far}} = 0, \quad V^{(ii)}_{yx,\mathrm{far}} = 0, \quad V^{(ii)}_{xx,\mathrm{near}} = -C/\sin^2(\pi y_i/W),$$
$$V^{(ii)}_{yy,\mathrm{near}} = V^{(ii)}_{xx,\mathrm{near}}, \quad V^{(ii)}_{xy,\mathrm{near}} = 0, \quad V^{(ii)}_{yx,\mathrm{near}} = 0,$$
$$V^{(ii)}_{\alpha\beta} = V^{(ii)}_{\alpha\beta,\mathrm{near}} + V^{(ii)}_{\alpha\beta,\mathrm{far}}.$$

For $i \neq j$,

$$X^- \equiv \pi(x_i - x_j)/(2W), \quad Y^\pm \equiv \pi(y_i \pm y_j)/(2W)$$

$$V^{(ij)}_{xx,\mathrm{far}} = C\frac{2\cos^2 Y^- \cosh^2 X^- - \cosh^2 X^- - \cos^2 Y^-}{(\cosh^2 X^- - \cos^2 Y^-)^2},$$

$$V^{(ij)}_{xy,\mathrm{far}} = 2C\frac{\cos Y^- \cosh X^- \sin Y^- \sinh X^-}{(\cosh^2 X^- - \cos^2 Y^-)^2},$$
$$V^{(ij)}_{yx,\mathrm{far}} = V^{(ij)}_{xy,\mathrm{far}}, \quad V^{(ij)}_{yy,\mathrm{far}} = -V^{(ij)}_{xx,\mathrm{far}},$$

$$V^{(ij)}_{xx,\mathrm{near}} = C\frac{2\cos^2 Y^+ \cosh^2 X^- - \cosh^2 X^- - \cos^2 Y^+}{(\cosh^2 X^- - \cos^2 Y^+)^2},$$

$$V^{(ij)}_{xy,\mathrm{near}} = -2C\frac{\cos Y^+ \cosh X^- \sin Y^+ \sinh X^-}{(\cosh^2 X^- - \cos^2 Y^+)^2},$$
$$V^{(ij)}_{yx,\mathrm{near}} = -V^{(ij)}_{xy,\mathrm{near}}, \quad V^{(ij)}_{yy,\mathrm{near}} = V^{(ij)}_{xx,\mathrm{near}},$$
$$V^{(ij)}_{\alpha\beta} = V^{(ij)}_{\alpha\beta,\mathrm{near}} + V^{(ij)}_{\alpha\beta,\mathrm{far}}.$$

For a given channel width W, Y^+ and Y^- are bounded from above and below. As $|X^-| \to \infty$ for fixed Y^+ and Y^-, the components of $\mathbf{V}^{(ij)}_{\alpha\beta}$ decay exponentially with screening length W/π or $2W/\pi$.

[1] H. W. Hou, A. A. S. Bhagat, A. G. L. Chong, P. Mao, K. S. W. Tan, J. Han, and C. T. Lim, Lab Chip **10**, 2605 (2010).
[2] M. J. Fuerstman, P. Garstecki, and G. M. Whitesides, Science **315**, 828 (2007).
[3] T. M. Schneider, S. Mandre, and M. P. Brenner, Phys. Rev. Lett. **106**, 094503 (2011).
[4] J. L. McWhirter, H. Noguchi, and G. Gompper, Proc. Natl. Acad. Sci. USA **106**, 6039 (2009).
[5] W. Lee, H. Amini, H. A. Stone, and D. D. DiCarlo, Proc. Natl. Acad. Sci. USA **107**, 22413 (2010).
[6] K. Drescher, K. C. Leptos, I. Tuval, T. Ishikawa, T. J. Pedley, and R. E. Goldstein, Phys. Rev. Lett. **102**, 168101 (2009).
[7] T. Beatus, T. Tlusty, and R. Bar-Ziv, Nature Phys. **2**, 743 (2006).
[8] M. Baron, J. Blawzdziewicz, and E. Wajnryb, Phys. Rev. Lett. **100**, 174502 (2008).
[9] A. Alvarez and R. Soto, Phys. Fluids **17**, 093103 (2005).
[10] Y. Or and R. M. Murray, Phys. Rev. E **79**, 045302(R) (2009).
[11] N. Liron and S. Mochon, J. Eng. Math. **10**, 287 (1976).
[12] H. Diamant, J. Phys. Soc. Jpn. **78**, 041002 (2009).
[13] T. Beatus, R. Bar-Ziv, and T. Tlusty, Phys. Rev. Lett. **99**, 124502 (2007).
[14] H. Aref, J. Roenby, M. A. Stremler, and L. Tophøj, Physica D **240**, 199 (2011).
[15] I. M. Janosi, T. Tel, D. E. Wolf, and J. A. C. Gallas, Phys. Rev. E **56**, 2858 (1997).
[16] C. M. Pooley, G. P. Alexander, and J. M. Yeomans, Phys. Rev. Lett. **99**, 228103 (2007).
[17] M. L. Ekiel-Jezewska and E. Wajnryb, Phys. Rev. E **83**, 067301 (2011).
[18] E. Evans and E. Sackmann, J. Fluid Mech. **194**, 553 (1988).